CHAPTER 2

Theory and Principle

2.1 Electron Source of the PBP-CMU Linac System

The PBP-CMU thermionic cathode electron gun consists of two TM_{010}-mode resonant cavities with the lengths of about half and full wavelength of the 2856 MHz radio-frequency (RF) wave, respectively. The RF wave is transmitted into the gun through a rectangular waveguide input-port located at the full-cell wall in vertical direction. The electromagnetic field is coupled from the full-cell to the half-cell through a side-coupling cavity, which is placed in horizontal direction. This leads the RF-gun to be a $\pi/2$-mode standing wave structure. The pictures of three-dimensional RF-gun model are illustrated in Fig. 2.1. In the gun operation, electrons are continuously emitted from the thermionic cathode located at the rear wall of the half-cell cavity and then are accelerated by the electric field component of the RF wave inside the cavity. Some electrons encountering a decelerating phase of the time-varying electric field are accelerated back to hit the cathode surface resulting in the electron back-bombardment effects, which leads to the instability of the gun operation. About one fourth of electrons emitted from the cathode are further accelerated in the second full-cell cavity and exit the gun with energies depending on the accelerating phase and electric field amplitude of the RF field.

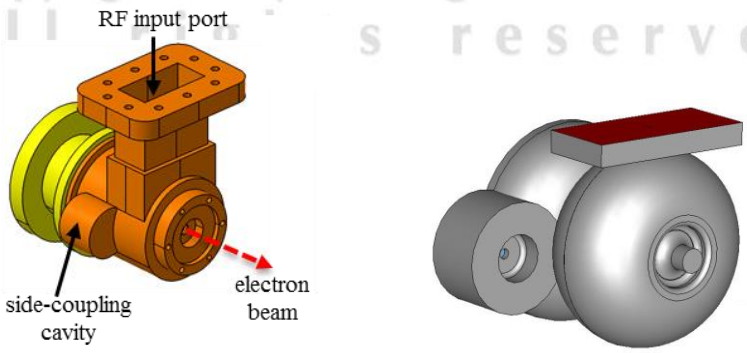

Figure 2.1: Outside and inside structures of the three-dimensional model of the PBP-CMU RF-gun [9].

A standing wave is the superposition of two equal waves moving in opposite directions. The RF waves travel back and forth in a cavity with the same velocity of the group velocity for a specific resonant frequency. The electron propagating in the cavity will be accelerated by the longitudinal electric field component and will have a final velocity depending on the accelerating phase and the amplitude of the RF field. The simplest and the most practical standing wave resonant cavity for electron acceleration is the TM_{010}-mode cylindrical resonant cavity, which has the electric field and magnetic field directions as illustrated in Fig. 2.2.

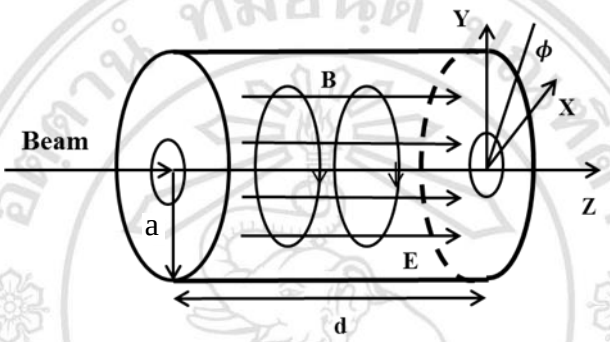

Figure 2.2: Electromagnetic field directions in the TM_{010}-mode pillbox cavity [10].

Consider wave equations of longitudinal electric and magnetic field propagating in free space, which are

$$\nabla^2 E_z + k^2 E_z = 0 \qquad \text{and} \qquad \nabla^2 B_z + k^2 B_z = 0\,, \tag{2.1}$$

where *k* is the wave number. When azimuthal symmetry and boundary condition at the cavity wall of $B_{\square} = B_{\perp} = 0$ are considered, the solution of the wave equations in terms of cylindrical coordinates (ρ, φ, z) and Bessel functions $J_m(k_c r)$ can be written as [11]

$$E_z(r,t) = E_0 J_0(k_c r)\cos\omega t\,, \tag{2.2}$$

$$B_\varphi(r,t) = -\frac{E_0}{c} J_1(k_c r)\sin\omega t\,. \tag{2.3}$$

As shown in Equations (2.2) and (2.3), ω is the angular resonant frequency of the wave, $k_c = 2\pi/\lambda_{rf}$ is the cutoff wavenumber, λ_{rf} is the wavelength of the wave and c is the velocity of light, which equals to $c = \omega/k_c$.

Equation (2.2) and (2.3) explain that the electromagnetic field components propagating inside the TM_{010}-mode pillbox cavity consist of only the longitudinal electric field (E_z) and the azimuthal magnetic field (B_φ). The amplitude of the longitudinal electric field is maximum at the radial center of the cavity and decreases down to zero at the conducting wall of the cavity, while the longitudinal electric field is constant throughout in z distance.

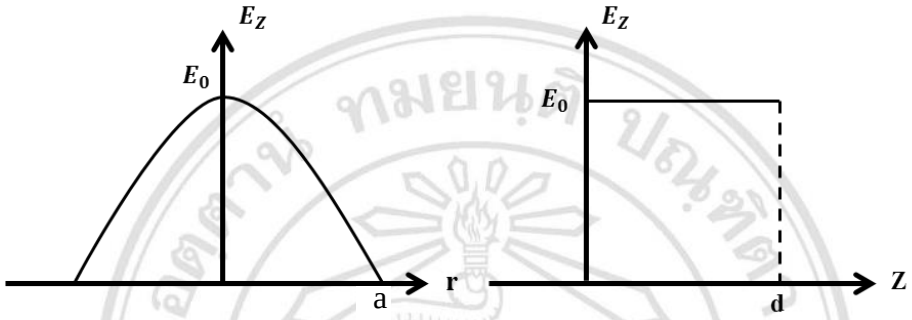

Figure 2.3: Longitudinal electric field (E_z) inside the TM_{010}-mode pillbox cavity as a function of the radius (r) and the longitudinal distance (z).

The fundamental frequency of the TM_{010}-mode cavity can be derived by considering the lowest zero value of the zero[th] order Bessel function $J_0(k_c r) = 0$ at $k_c r = 2.405$. The fundamental frequency or the resonant frequency (f_{rf}) of the cavity depends on the cavity radius (a) as

$$f_{rf} = \frac{\omega}{2\pi} = \frac{ck_c}{2\pi\sqrt{\mu\varepsilon}} = \frac{2.405c}{2\pi\sqrt{\mu\varepsilon}\,a}, \tag{2.4}$$

where μ and ε are the relative permeability and permittivity of the medium in the cavity, respectively. Normally, the medium of the cavity is vacuum with $\mu = \varepsilon = 1$. Thus, the radius of the TM_{010}-mode pillbox cavity is given by

$$a = 2.405\frac{c}{2\pi f_{rf}}. \tag{2.5}$$

A relativistic electron with the velocity close to the light velocity must travel through the resonant cavity of length *d* within a half of an RF period for the most efficient acceleration. Therefore, the cavity length of the TM_{010}-mode cavity becomes

$$d = \frac{\beta c T_{rf}}{2} = \frac{\beta c}{2 f_{rf}} = \frac{\beta \lambda_{rf}}{2}, \tag{2.6}$$

where T_{rf} is the RF period, λ_{rf} is the RF wavelength and $\beta = v/c$ when v is the velocity of the electron.

The time varying longitudinal electric field of the TM_{010}-mode can be written as

$$E_z(z,t) = E_0 \cos(\omega t + \varphi), \tag{2.7}$$

where E_0 is the electric field amplitude and φ is the initial phase different. An energy gain (ΔE_{gain}) of the electron beam and an accelerating voltage (V_{acc}) of the resonant cavity can be calculated from the longitudinal electric field in the cavity length of *d* as

$$\Delta E_{gain} = e \int_{-d/2}^{d/2} E_0 \cos(\frac{\omega z}{v}) dz = eV_{acc}, \tag{2.8}$$

$$V_{acc} = \int_{-d/2}^{d/2} E_0 \cos(\frac{\omega z}{v}) dz = \frac{2vE_0}{\omega} \sin\left(\frac{\omega d}{2v}\right) = E_0 d T_f, \tag{2.9}$$

where T_f is the transit time factor, which is given by

$$T_f = \frac{\sin(\omega d / 2v)}{\omega d / 2v}. \tag{2.10}$$

When the electron is accelerated at the accelerating phase of $\pi/2$, it gains a maximum energy from the field and the transit time factor becomes

$$T_f = \frac{\sin(\pi / 2)}{\pi / 2} = \frac{2}{\pi}. \tag{2.11}$$

Therefore, the maximum accelerating voltage equals to $V_{acc} = 2E_0 d/\pi$ and the average electric field experienced by the electron traveling across the resonant cavity is

$$E_{ave} = \frac{V_{acc}}{d} = \frac{2E_0}{\pi}.$$

(2.12)

The time-dependent magnetic field component of the RF wave encountering with a non-perfect conducting cavity wall, which has a finite resistance, induces surface currents in the cavity wall. These induced currents cause RF power loss to the conducting surface and result in heating up of the cavity wall. The penetration of the RF field into the wall of the resonant cavity is limited by the skin depth (δ_s) of the cavity as

$$\delta_s = \sqrt{\frac{2}{\mu_0 \sigma_s \omega}}, \tag{2.13}$$

where μ_0 is the vacuum permeability and σ_s is the conductivity of the cavity material. The cavity wall losses or the power dissipation (P_{cy}) depends on the accelerating voltage and the cavity shunt impedance (R_s) defined by

$$P_{cy} = \frac{V_{acc}^2}{R_s} = \frac{V_{acc}^2}{r_s d}, \tag{2.14}$$

$$R_s = \frac{4\pi\varepsilon_0}{\sigma_s \delta_s},$$

(2.15)

where r_s is the shunt impedance per unit length of the cavity and ε_0 is the vacuum permittivity. The shunt impedance depends greatly on the cavity geometry and the quality of the material surface.

A quality factor (Q-factor) implies to the accelerating efficiency of the electron in the cavity with specific resonant frequency. It can be written in terms of stored field energy (U) in the cavity and the dissipated power per RF cycle as

$$Q = \frac{2\pi U}{T_{rf} P_{cy}} = \frac{\omega U}{P_{cy}}. \tag{2.16}$$

A higher Q-factor value provides larger stored energy. The stored energy can be evaluated from a volume integral of the squared longitudinal electric field as

$$U = \frac{\varepsilon_0}{2} \int_V \left| E^2 \right| dV \,. \tag{2.17}$$

2.2 Travelling-wave Linear Accelerator

A SLAC-type S-band traveling-wave linear accelerator (linac) is employed to increase the kinetic energy of electron beam after exiting the alpha magnet. The linac structure is called a disk-loaded cylindrical waveguide, which has a series of conducting disks with central hole. A typical disk-load linac structure is shown in Fig. 2.4. The typical SLAC-type linac is operated in 2π/3-mode, which the axial electric field has the phase difference of 2π/3 between two adjacent accelerating cells as shown in Fig. 2.5. The main advantages of this mode include high group velocity and large shunt impedance [12].

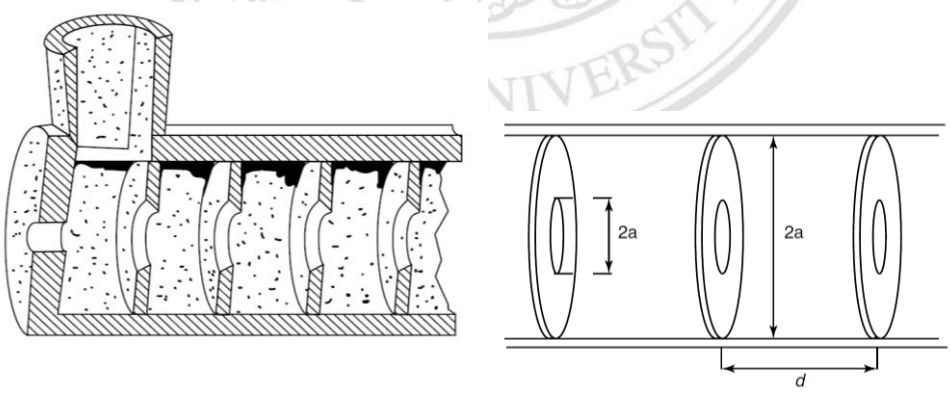

Figure 2.4: Disk-loaded traveling-wave structure with waveguide input port [13].

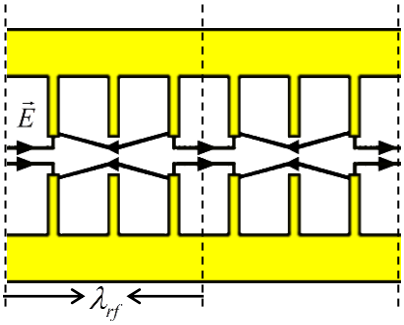

Figure 2.5: Schematic picture shows the $2\pi/3$ operating mode of traveling-wave linac acceleration. The electric field has a phase shift of $2\pi/3$ per cavity [13].

There are two main categories of the travelling-wave linac; a constant-gradient structure and a constant-impedance structure. The PBP-CMU Linac discussed in this thesis has constant gradient structure, which the cavity apertures and the iris holes in the disks are getting smaller along the linac section [14]. The RF wave propagates simultaneously with the electron bunch in one direction throughout the accelerating structure. The wave is terminated with the matched resistive load at the end of the linac while the electrons travel further with the velocities corresponding to their kinetic energies. The energy gain per linac section with a length of 10 ft (3.048 m) is

$$\Delta E_{kin} = eV_0 = e\int_0^L E_z dz = e\sqrt{r_S L P_0}\sqrt{1-e^{-2\tau}}\cos\psi_s,$$

(2.18)

where L is the length of the linac, τ is the attenuation factor and ψ_s is the synchronous phase that the electron travels with the RF field. A numerical calculation shows that the SLAC linac structure has an energy gain per section (10 ft) of [14]

$$\Delta E_{kin}[MeV] = 10.48\sqrt{P_0[MW]}, \qquad (2.19)$$

where P_0 is the RF pulse power supplied to the linac.

2.3 Charged Particle Motion in Electromagnetic Fields

Besides the acceleration due to longitudinal electric field component in the RF electron gun and the linac, the electron beam also experiences transverse magnetic

fields from various magnets. The electric and magnetic forces acting on a charged particle with electric charge q can be written as

$$\vec{F} = q\left(\vec{E} + \vec{v} \times \vec{B}\right), \tag{2.20}$$

Equation (2.20) is called the Lorentz force. Consider that the charged particle described in this section is a positive charged particle with the electric charge of $q = e$. This equation reveals that both transverse electric and magnetic field can be used to deflect a charged particle, but the magnitude of the electric field is v/c times higher than the magnetic field for the same radius of a curvature trajectory. Consequently, the transverse magnetic field is popularly employed to adjust the particle trajectory and to control the transverse beam size in a high energy accelerator. It is noted that a magnetic force occurs only for a moving charged particle.

The positive charge motion in the accelerator system can be described with respect to a reference trajectory, which is a designed path for the particle passing through the beamline as shown in Fig. 2.6. To obtain the equation of motion in the transverse magnetic field, Newton's law and the Lorenz force are considered to be equal as

$$\vec{F} = \gamma m_0 \ddot{\vec{r}} = e\left(\vec{v} \times \vec{B}\right), \tag{2.21}$$

where m_0 is the rest mass of charged particle and $\ddot{\vec{r}}$ represents the particle acceleration in terms of the second derivative of the displacement vector ($\vec{r} = s\hat{s} + x\hat{x} + y\hat{y}$) with respect to time. Here, s is the longitudinal coordinate and (x, y) are transverse coordinates of the particle. The particle velocity is defined in terms of the velocities in each axis as $\vec{v} = v_x\hat{x} + v_y\hat{y} + v_s\hat{s}$. The transverse magnetic field is determined as $\vec{B} = B_x\hat{x} + B_y\hat{y}$.

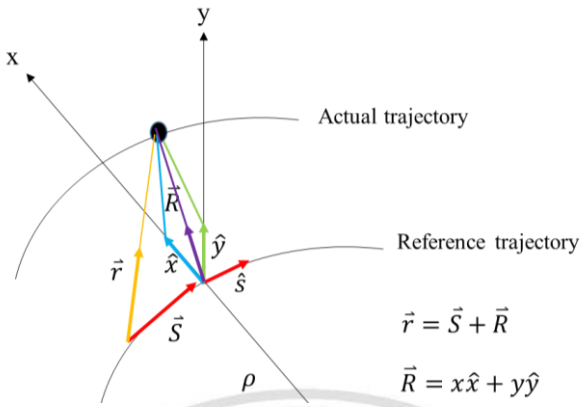

Figure 2.6: Actual path of a positive charge e with respect to the reference trajectory [15].

Thus, the equations of motion in x and y directions in term of the derivatives with respect to time are

$$\ddot{x} - \left(1 + \frac{x}{\rho}\right)\frac{\dot{s}^2}{\rho} = -\left(\frac{e}{\gamma m_0}\right)v_s B_y \qquad \text{and} \qquad \ddot{y} = \left(\frac{e}{\gamma m_0}\right)v_s B_x ,$$

(2.22)

where ρ is the curvature radius of the particle deflection. These equations will be changed to be the differential equations in term of the derivatives with respect to the longitudinal coordinate s by substituting $v_s = \left(1 + (x/\rho)\right)\dot{s}$ and by using the chain rule, which are $\dot{x} = x'\dot{s}$, $\ddot{x} = \dot{s}^2 x''$, $\dot{y} = y'\dot{s}$ and $\ddot{y} = \dot{s}^2 y''$. In addition, the transverse velocities are assumed to be very small compared to the longitudinal velocity. Thus, the electron velocity can be estimated to be equal to the velocity in the longitudinal direction or $v = \sqrt{v_x^2 + v_y^2 + v_s^2} \approx v_s$. Consequently, the equations of motion in term of the derivatives with respect to the longitudinal coordinate for the electron deflected in x axis by the transverse magnetic field become

$$x'' - \frac{1}{\rho}\left(1 + \frac{x}{\rho}\right) = -\frac{eB_y}{p}\left(1 + \frac{x}{\rho}\right)^2 \qquad \text{and} \qquad y'' = \frac{eB_x}{p}\left(1 + \frac{x}{\rho}\right)^2 , \qquad (2.23)$$

when $\gamma m_0 v$ is replaced by the particle momentum p. On the other hand, the equations of motion for the particle deflected in y axis by the transverse magnetic field are

$$x'' = \frac{qB_y}{p}\left(1+\frac{x}{\rho}\right)^2 \qquad \text{and} \qquad y''-\frac{1}{\rho}\left(1+\frac{y}{\rho}\right) = -\frac{qB_x}{p}\left(1+\frac{y}{\rho}\right)^2. \tag{2.24}$$

The transverse magnetic fields can be expressed in terms of multipole expansion by using the Taylor's expansion as

$$B_x(x,y) = B_{xo} + \frac{\partial B_x}{\partial x}x - \frac{\partial B_x}{\partial y}y + \frac{1}{2}\frac{\partial^2 B_x}{\partial x^2}(x^2-y^2) + \frac{\partial^2 B_x}{\partial x \partial y}xy + \ldots,$$

(2.25)

$$B_y(x,y) = B_{yo} + \frac{\partial B_y}{\partial x}x - \frac{\partial B_y}{\partial y}y + \frac{1}{2}\frac{\partial^2 B_y}{\partial x^2}(x^2-y^2) + \frac{\partial^2 B_y}{\partial x \partial y}xy + \ldots, \tag{2.26}$$

where the zero[th], the 1[st] and the 2[nd] order terms represent magnetic field components of dipole, quadrupole and sextupole magnets, respectively. Eventually, the equations of motion of the charged particle in the external transverse magnetic fields for all magnets can be written in a general form as

$$x''+k_x^2 x = 0 \qquad \text{and} \qquad y''-k_y^2 y = 0,$$

(2.27)

where k_x and k_y are specified by the components of the transverse magnetic field for the considered magnets. These well-known equations are called Hill's equation, which is used to explain betatron oscillation of the particle path around the reference trajectory. The equations of motion in Equation (2.27) can be solved if we know the magnetic field parameters. However, computer programs were used to simulate the particles' motion in electromagnetic fields for all components considered in this study for convenience and fast optimization.

In this thesis, we used three types of magnet in beam dynamic simulation, which are steering magnets, quadrupole magnets and an alpha magnet. Brief explanation of each magnet type is described as follow.

2.3.1 Steering Magnet

A steering magnet is a small dipole magnet, which is used to correct the transverse direction of the electron beam to a desired position. The steering magnets at

the PBP-CMU Linac Laboratory consists of a rectangular iron yoke with four conducting coils. A picture and a schematic structure of the steering magnet is displayed in Fig. 2.7. Two power supplies are connected to the conducting coils for separately driving each pair of coils. In this case, we can bend the beam in both horizontal and vertical directions at the same location.

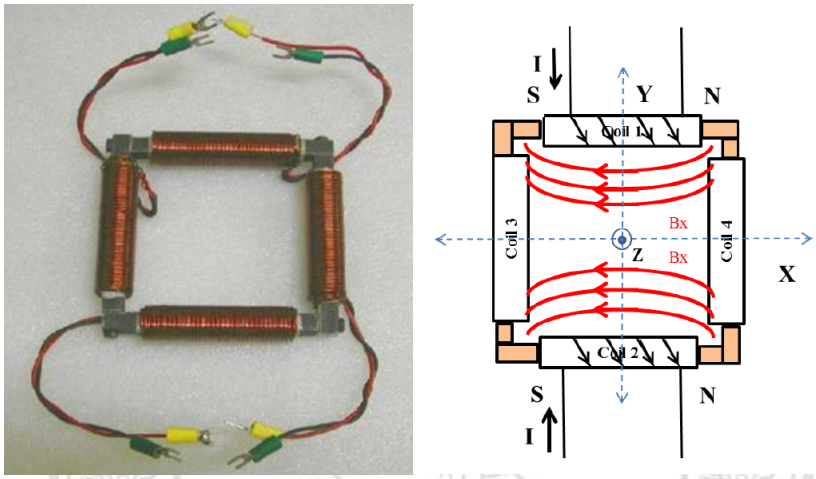

Figure. 2.7: Picture of the steering magnet at the PBP-CMU Linac Laboratory (left) and a schematic structure of the steering magnet illustrating the magnetic field lines, which can be employed as a vertical bending magnet (right) [16].

From the magnetic field measurement, the transverse magnetic fields increase exponentially from the magnet axis to the conducting coils in all four sides and decrease exponentially from the center to both sides along the z direction [17]. The effective length (l_{eff}) of the steering magnet can be evaluated from

$$l_{eff} = \frac{\int Bdz}{B_0}, \tag{2.28}$$

where B is the transverse magnetic field in x or y directions and B_0 is a magnitude of the transverse magnetic field at the centroid of the magnet. The bending radius ρ of the steering magnet can be calculated from the practical formula as [14]

$$\frac{1}{\rho[m]} = 0.2998\frac{B[T]}{\beta E[GeV]}, \tag{2.29}$$

where $\beta = v/c$ is the ratio of particle velocity and the light velocity and E is the total energy of particle. Thus, the deflecting angle α can be obtained from

$$\alpha = \frac{l_{eff}}{\rho}\ , \tag{2.30}$$

2.3.2 Quadrupole Magnet

A quadrupole magnet composes of four magnetic poles, conducting coils of N turn and an iron yoke. The opposite poles of the magnet have the same magnetic polarity. An aperture between each pole face equals to 2*R*, where *R* is the bore radius of the quadrupole aperture as illustrated in Fig. 2.7. The charged particle beam moving through the quadrupole will be focused in a direction and defocused in another direction. The magnetic field strength inside the aperture increases linearly from the centroid of the magnet close to the pole face of the quadrupole.

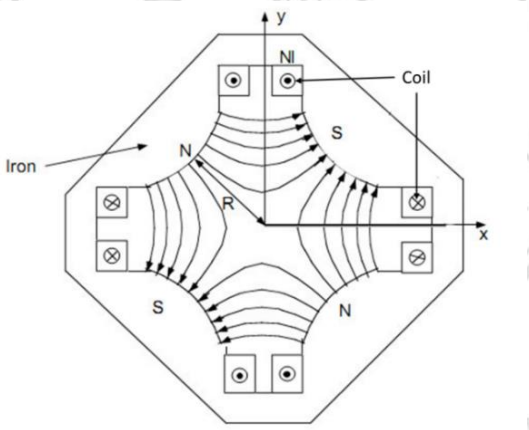

Figure. 2.8: Cross sectional structure of a quadrupole magnet [18].

The transverse magnetic field of the quadrupole magnet is linearly increased when the distance from the magnet center increases. Hence, the magnetic field gradient (g) of the quadrupole magnet is constant, which can be expressed by

$$g = \frac{2\mu_0 IN}{R^2}\,. \tag{2.31}$$

A magnetic field strength of the quadrupole is defined as

$$k = \frac{qg}{p} = \frac{1}{fl_{eff}}, \tag{2.32}$$

where q is the charge of moving particle, p is the particle momentum, f is the focal length of the quadrupole and l_{eff} is the effective length, which can be calculated by

$$l_{eff} = \frac{\int g dz}{\langle g \rangle}, \tag{2.33}$$

where $\langle g \rangle$ is the average magnetic gradient close to the center of the quadrupole. The practical formula for convenient calculation of the quadrupole strength [14] is

$$k[m^{-2}] = 0.2998 \frac{g[T/m]}{\beta E[GeV]}, \tag{2.34}$$

2.3.3 Alpha Magnet

An alpha magnet is used as a bunch compressor for low-energy electron beam with well correlation between the energy and time. Electrons with different kinetic energies travel in the alpha magnet magnetic field with different path lengths. Lower energy electrons with shorter travelling path lengths catch up with higher energy electrons at the desired position downstream the alpha magnet. The alpha magnet is also employed as an energy filter. High and low energy slits located inside the vacuum chamber of the alpha magnet are used to select the electron beam with desired energy range to decrease energy spread and bunch length before the beam is further accelerated in the linac. Furthermore, the energy spectrum of electron beam can be measured by using the alpha magnet energy slits.

The alpha magnet has a shape of half quadrupole magnet with a metal mirror plate [19]. In the alpha magnetic field, an electron follows a trajectory with an α-like shape and departs from the magnet at the same position of the entrance but with different angle of 81.42^{o} as illustrated in Fig. 2.9. Thus, the space charge effect in the alpha magnet is greatly complicate due to the couple of transverse and longitudinal motions [19]. The maximum distances in horizontal, vertical and longitudinal directions of the electron trajectory inside the alpha magnet can be written as [20]

$$x_{\max}(cm) = 75.051\sqrt{\frac{\beta\gamma}{g(G/cm)}}, \tag{2.35}$$

$$y_{\max}(cm) = 24.620\sqrt{\frac{\beta\gamma}{g(G/cm)}}, \tag{2.36}$$

$$s_{\max}(cm) = 191.655\sqrt{\frac{\beta\gamma}{g(G/cm)}}, \tag{2.37}$$

where $s_{\max}$ represents the electron path length inside the alpha magnet, g is the gradient of the alpha magnet and the Lorentz factor (γ) corresponds to the total energy in term of the electron rest mass energy.

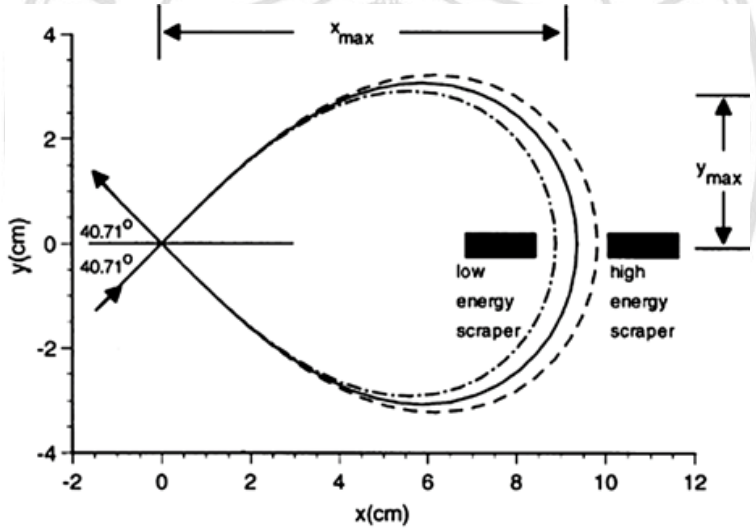

Figure 2.9: Electron trajectories in the alpha magnet with energy slits [6].

2.4 Electron Beam Parameters

2.4.1 Time Structure

The electron beam produced from the PBP-CMU Linac system is a bunch beam, which each bunch is divided with a time duration depending to the resonant frequency of the RF wave. In our case, the resonant frequency of the RF wave for both RF-gun and linac is 2856 MHz. Thus, the electron bunches are separated with the RF period

(τ_{rf}) of 350.14 ps. A group of electrons in the bunch corresponding to the above definition is popularly called a micro-bunch. The length of each micro-bunch is represented by $\delta\tau$ as shown in Fig. 2.10.

Typically, the RF systems of the PBP-CMU Linac system produce the RF pulses at a repetition rate of 10 Hz. A repetition time or a time interval between each RF pulse can be calculated from the repetition rate. The shape and length of the RF pulse depend on performance of the modulator system and the Pulse Forming Network (PFN) system. A train of electron micro-bunches is called a macro-pulse. Since the RF power systems of the PBP-CMU RF-gun and linac are operated at the repetition rate of 10 Hz. Thus, the time interval of the macro-pulse (τ_{rep}) is 100 ms as shown in Fig. 2.10.

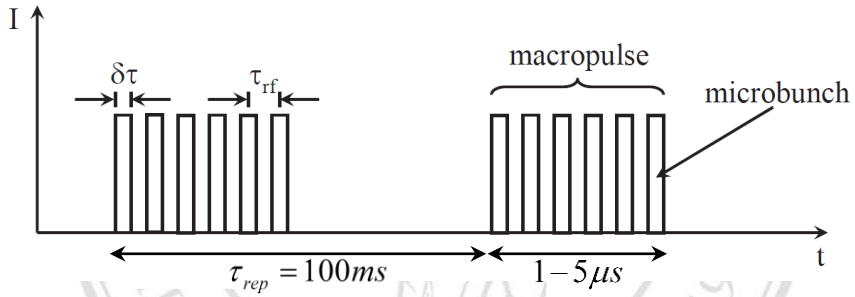

Figure. 2.10: Time structure of the electron beam modified from the reference [5].

2.4.2 Beam Currents

An electron beam current can be specified in different definitions. The current of the micro-bunch is named a peak current (I_{peak}). It is defined in terms of the micro-bunch charge (q_b) and the bunch length ($\delta\tau$) as shown in the following equation.

$$I_{peak} = \frac{q_b}{\delta\tau}. \tag{2.38}$$

A pulse current (I_{pulse}) for a train of N_b micro-bunches can be calculated from a total charge (Q_p) in a macro-pulse divided by a period length of each pulse (τ_p) as

$$I_{pulse} = \frac{Q_p}{\tau_p} = \frac{N_b q_b}{N_b \tau_{rf}} = \frac{q_b}{\tau_{rf}} .$$

(2.39)

An average current (I_{ave}), which is crucial in most experiments, is defined in terms of a total charge (Q) and a considered time during the experiment. Practically, the average current can be calculated per second and it is expressed by

$$I_{ave} = \frac{Q}{t} = \frac{Q_p}{\tau_{rep}} = \frac{N_b q_b}{\tau_{rep}} . \quad (2.40)$$

2.4.3 Electron Beam Energy and Energy Spread

Electrons in the micro-bunch are accelerated in the RF-gun and the linac with different RF phases. They gain different energies from the longitudinal electric field due to the time-dependent field characteristics. This leads to an energy deviation or energy spread (δE) of the beam. In numerical calculation, this value can be evaluated from a standard deviation of the electron energy as

$$\Delta E = \frac{1}{N_e} \sqrt{\Sigma \left(E_e - E_{av} \right)^2} ,$$

(2.41)

where N_e is the number of electrons in the micro-bunch, E_e is the individual electron energy and E_{av} is the average energy of the electron bunch.

2.4.4 Transverse Beam Emittance

Transverse beam emittance (ε) corresponds to an area in phase space ellipse of the electron beam transverse distribution as shown in Fig. 2.11. The phase space ellipse can be described with the beam emittance and twiss parameters (α, β, γ). According to Fig. 2.11, the quantity $\sqrt{\varepsilon\beta}$ is equal to half of the beam width, $\sqrt{\varepsilon\gamma}$ specifies converging or diverging angles of the beam, $\sqrt{\varepsilon/\beta}$ presents the vertical intersection and $\sqrt{\varepsilon/\gamma}$ is the horizontal intersection.

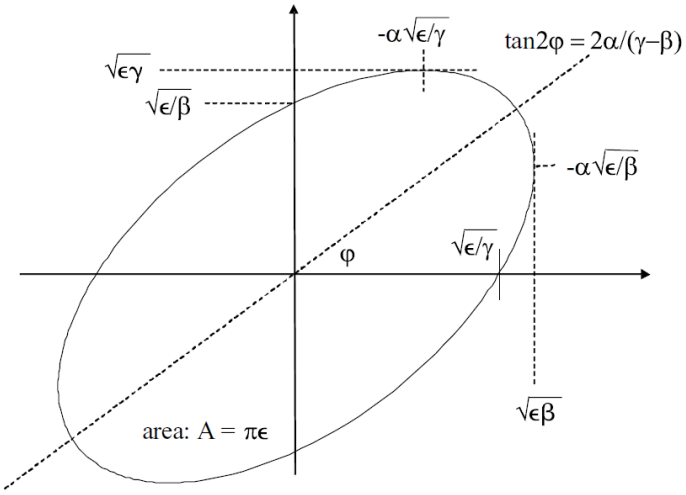

Figure 2.11: Phase space ellipse with betatron function of an electron bunch [14].

In numerical calculation, an RMS transverse emittance $(\varepsilon_{x.rms}, \varepsilon_{y.rms})$ can be evaluated from the transverse displacements (x_i, y_i) and the angular displacements (x_i', y_i') of electrons in the bunch as [21]

$$\varepsilon_{x,rms} = \sqrt{\left\langle \left(x_i - \langle x_i \rangle\right)^2 \right\rangle \left\langle \left(x_i' - \langle x_i' \rangle\right)^2 \right\rangle - \left\langle \left(x_i - \langle x_i \rangle\right)\left(x_i' - \langle x_i' \rangle\right) \right\rangle^2}\,, \tag{2.42}$$

$$\varepsilon_{y,rms} = \sqrt{\left\langle \left(y_i - \langle y_i \rangle\right)^2 \right\rangle \left\langle \left(y_i' - \langle y_i' \rangle\right)^2 \right\rangle - \left\langle \left(y_i - \langle y_i \rangle\right)\left(y_i' - \langle y_i' \rangle\right) \right\rangle^2}\,. \tag{2.43}$$

These equations can be used for the electron bunch with all transverse distributions. The angular displacements are defined by $x_i' \approx p_x / p_z$ and $y_i' \approx p_y / p_z$, where p_x, p_y, p_z are electron momenta in each direction. We can estimate $p_z \approx p$ for very small transverse momenta compared to longitudinal momentum ($p_x, p_y \ll p_z$). Furthermore, a normalized emittance (ε_n) can be derived from the RMS emittance and the beam energy. This emittance value is very useful for comparison of electron beams with different energies. The normalized emittance is given by

$$\varepsilon_n = \beta\gamma\varepsilon_{rms}\,. \tag{2.44}$$

2.5 Space Charge Effects

Electric and magnetic self-fields produced from each electron within a bunch are related to the space charge field. The electric self-field leads to the repulsion of the electrons by the Coulomb force, which is close to zero at the beam center and increases to maximum value near the boundary of the beam. The magnetic self-field is created from moving electrons and causes radial attractive forces in the bunch. The total effect of the electron self-fields depends greatly on the energy of the electron beam. The Lorentz force in the radial direction due to the self-fields can be written as [22]

$$F(r) = qE_r\left(1-\beta^2\right) = \frac{qE_r}{\gamma^2}, \tag{2.45}$$

where E_r is a radial component of the electric self-field. The term qE_r in the equation represents the electric self-force and the term $qE_r\beta^2$ is the magnetic self-force. The absolute cancellation of both forces appears as the electron velocity close to the speed of light. The radial electric field depends on the distribution of the beam density. For a Gaussian beam density of $\rho(r) = \rho_0 \exp\left(-r^2/2\sigma_r^2\right)$ with a standard deviation of σ_r, the space charge electric field can be expressed by [22]

$$E_r(r) = \frac{\rho_0\sigma_r^2}{\varepsilon_0 r}\left[1-\exp\left(\frac{-r^2}{2\sigma_r^2}\right)\right], \tag{2.46}$$

where ρ_0 is the maximum charge density. The redial space charge field affects the transverse properties of the electron beam. The larger space charge field leads to the larger transverse beam size and divergence resulting in the emittance growth.

2.6 Beam Dynamic Simulation

In this thesis, two simulation programs were used to study the beam dynamics of electrons travelling in the accelerator system. Short description of the two programs, which are program PARMELA and program ELEGANT, are summarized as follow.

2.6.1 PARMELA

The program PARMELA (Phase And Radial Motion in Electron Linear Accelerator) was employed to simulate the electron beam dynamics and investigate the optimum electron beam properties in all components in the accelerator system except in the alpha magnet. PARMELA is a particle-in-mesh code that simulates the dynamics of macro-particle in the electromagnetic field distributions of the accelerator components by solving Maxwell's equations. It is capable to track macro-particles through magnetic elements and other transport components including space charge effect calculation. However, it cannot be used with the alpha magnet [23].

Several electron emission distributions are possible to be specified in the input file of the program PARMELA. In our case, we used the transverse and longitudinal uniform distributions. An external 3D electromagnetic field distribution of the RF-gun can be imported to the PARMELA simulation. A hard-edge quadrupole magnet and a zero-length steering magnet are utilized in this code. The space charge field is not calculated in the steering magnetic field. A traveling-wave accelerator is specified by several parameters, which are an RF phase, a resonant frequency, an average axial electric field, a phase shift per cell, and accelerating cell dimensions. The electromagnetic field of the traveling-wave linac is produced from the field expansion in the Fourier-Bessel series and a sinusoidal wave is used for defining the RF phase of the linac. Thus, the electron will gain maximum energy at the on-crest phase of the RF wave, which is equal to 90°.

The 2D space charge field was employed in the space charge mesh calculation in this study. Proper mesh intervals in radial and longitudinal directions were defined. The results of mesh interval optimization are presented in Chapter 3. The coordinates and momenta of the macro-particles, which are represented a group of electrons in a bunch,

are transformed to the rest frame and are considered to be infinitesimally thin rings in a rectangular area of the mesh interval as displayed in Fig. 2.12. The space charge field is calculated by using the elliptic integrals and the impulses are delivered back to all macro-particles within the bunch.

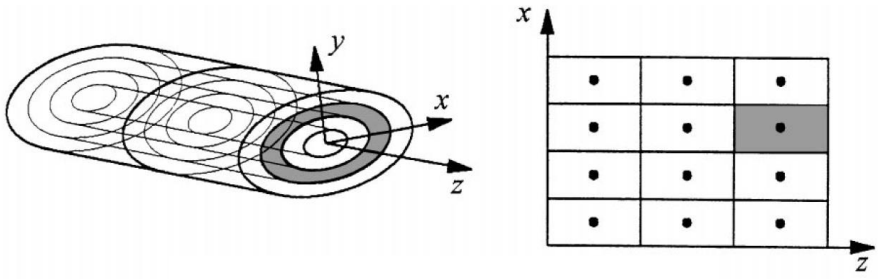

Figure 2.12: Elliptical model of macro-particles in an electron bunch (left) and the rectangular cross-section of the elliptical model (right) [24].

2.6.2 ELEGANT

The ELEGANT (ELEctron Generation ANd Tracking) program is used to simulate beam optics and beam transportation of macro-particles along various elements of the accelerator system. It calculates the particles' motion via the transport matrices. The first order transport matrices are utilized for linear beam dynamic simulation while the higher order matrices are used for non-linear beam dynamic simulation.

In this study, we used the program ELEGANT for the calculation in steering, quadrupole and alpha magnets. The steering magnet in the code ELEGANT is a time-independent kicker and is a rectangular dipole model with no fringe field effect. It has a combination of horizontal and vertical magnetic field strengths that are defined by the kick angles. A quadrupole magnet is a hard-edge model and has constant magnetic field along its effective length. Instead of describing in term of magnetic field, an alpha magnet's gradient (g) is specified by a parameter call "*xmax*", which is given by Equation (2.35).

This code generally excludes the space charge effect in the calculation. Nevertheless, both longitudinal and transverse space charge calculation are capable to be applied in the simulation representing by the space charge kick element, which must be inserted after all elements in the transport line. Therefore, the space charge

simulation in ELEGANT cannot be included in transport matrix of each component in the accelerator system. Furthermore, it is not available for the RF-gun and linac simulation [25].

2.7 Undulator Magnet and Undulator Radiation

One of the main parts of my study is the investigation of the coherent undulator radiation. Thus, some principles and theories related to the electron motion in undulator magnetic field and the undulator radiation are included in this section.

2.7.1 Electron Motion in Undulator Magnetic Field

Typical undulator magnets compose of a periodic structure of dipole magnets with opposite polarity arrangement between each dipole. For simplicity, we assume that the width in horizontal direction of the magnet pole is equal to infinity or much larger than a period length (λ_u) of the undulator. Thus, the magnetic fringe field at the edge of the poles is excluded from this consideration and the horizontal magnetic field component can be neglected. A static magnetic field (B_y) described in Equation (2.47) is alternating in vertical direction throughout the length of the undulator as [26]

$$B_y(z) = \tilde{B}\sin\left(\frac{2\pi z}{\lambda_u}\right), \tag{2.47}$$

where $\tilde{B}$ is the peak magnetic field of the undulator magnet, which correlates to the magnetic field B_0 in the mid plane $(\mathrm{x}=0, \mathrm{y}=0)$ as

$$\tilde{B} = \frac{B_0}{\cosh\left(\frac{\pi g}{\lambda_u}\right)}. \tag{2.48}$$

Equation (2.48) indicates that the peak magnetic field can be varied by changing the period length and the pole gap. In practice, the undulator period length is usually

defined. Therefore, the peak magnetic field decreases when the pole gap increases. For the electromagnetic undulator, the peak magnetic is easily changed by adjusting the applied electric current to the conducting coils.

Relativistic electrons moving through the periodic field of the undulator are oscillating in the transverse direction and emitting the radiation with the radiation wavelength corresponding to the electron energy and the undulator parameters. Schematic picture of undulator radiation is shown in Fig. 2.13.

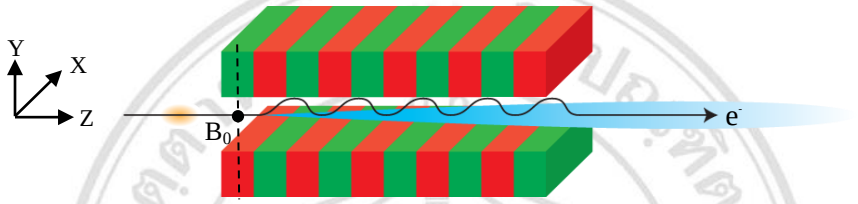

Figure 2.13: Schematic picture illustrates the sinusoidal trajectory of the electron along the undulator axis with the emitted radiation [27].

The motion of electron in the undulator magnetic field can be derived by considering the second differential equation of motion and the Lorentz force as

$$\vec{F} = \gamma m_0 \ddot{\vec{r}} = -e\left(\dot{\vec{r}} \times \vec{B}\right), \tag{2.49}$$

where the electron's displacement is $\vec{r} = x\hat{x} + y\hat{y} + z\hat{z}$. Since the vertical velocity of the electron and the horizontal magnetic field are ignored in this consideration, the transverse and longitudinal acceleration can be expressed by two couple equations as [26]

$$\ddot{x} = \frac{e}{\gamma m_0} B_y \dot{z}, \tag{2.50}$$

and

$$\ddot{z} = -\frac{e}{\gamma m_0} B_y \dot{x}. \tag{2.51}$$

For a relativistic electron with longitudinal velocity much larger than the transverse velocity ($v_z \approx c$ $\dot{x}$), the longitudinal velocity can be considered to be constant. Here, β_z is the longitudinal velocity of the particle with respect to the velocity of light. The second derivative with respect to time can be changed to the second derivative with respect to longitudinal displacement by using the chain rule. Then, we obtain

$$\ddot{x} = \frac{d\dot{x}}{dt} = \frac{d\dot{x}}{dz}\frac{dz}{dt} = \frac{d}{dz}\left(x'\dot{z}\right)\dot{z} = x''\dot{z}^2 ,$$

(2.52)

and we get $$x''(z) = \frac{e\tilde{B}}{\gamma m_0 \beta_z c}\sin\left(\frac{2\pi z}{\lambda_u}\right).$$

(2.53)

Integrating Equation (2.53) and substituting the initial condition as $x'(0) = e\tilde{B}\lambda_u / 2\pi\gamma m_0 \beta_z c$. A deflecting angle ($\alpha_{deflect}$) from the average trajectory is then written as

$$\alpha_{deflect}(z) = x' = \frac{e\tilde{B}\lambda_u}{2\pi\gamma m_0 \beta_z c}\cos\left(\frac{2\pi z}{\lambda_u}\right) = \frac{K}{\gamma\beta_z}\cos\left(\frac{2\pi z}{\lambda_u}\right).$$

(2.54)

An undulator parameter $K = e\tilde{B}\lambda_u / 2\pi m_0 c = 0.934\tilde{B}[T]\lambda_u[cm]$ is the dimensionless variable, which describes the deflecting strength of electron motion in the undulator magnetic field. Integrating Equation (2.54) and substituting the initial condition $x(0) = 0,$ we will get the electron displacement (x_{dist}) along the undulator axis as

$$x_{dist}(z) = \frac{e\tilde{B}\lambda_u^2}{4\pi^2\gamma m_0 \beta_z c}\sin\left(\frac{2\pi z}{\lambda_u}\right) = \frac{K\lambda_u}{2\pi\gamma\beta_z}\sin\left(\frac{2\pi z}{\lambda_u}\right).$$

(2.55)

This equation refers to the sinusoidal trajectory of electron in the x-z plane as shown in Fig. 2.14. The maximum deflecting angle ($\alpha_{deflect,max}$) of the electron trajectory with respect to the undulator axis is

$$\alpha_{deflect,max} = x'_{max} = \frac{K}{\gamma\beta_z} \approx \frac{K}{\gamma}.$$

(2.56)

The main feature of the undulator magnet compared to the wiggler magnet is that it has weaker magnetic field with smaller undulator parameter as $K \leq 1$. Then, the maximum deflecting angle becomes $\alpha_{deflect,max} \leq 1/\gamma$, which relates to a narrow cone of the synchrotron radiation with a half opening angle of $\pm 1/\gamma$. The radiation cone is located around the tangent of the electron orbit that is closely parallel to the z direction. In contrast, the maximum angle larger than $1/\gamma$ corresponds to the magnet with undulator parameter of more than 1.

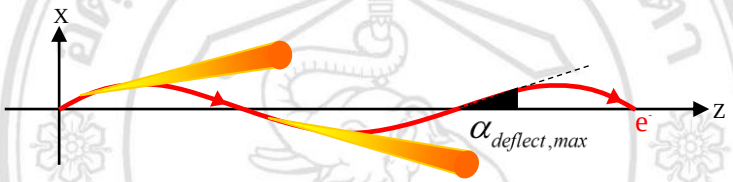

Figure 2.14: Electron moving path in the undulator magnetic field with its radiation cone [26].

2.7.2 Undulator Radiation

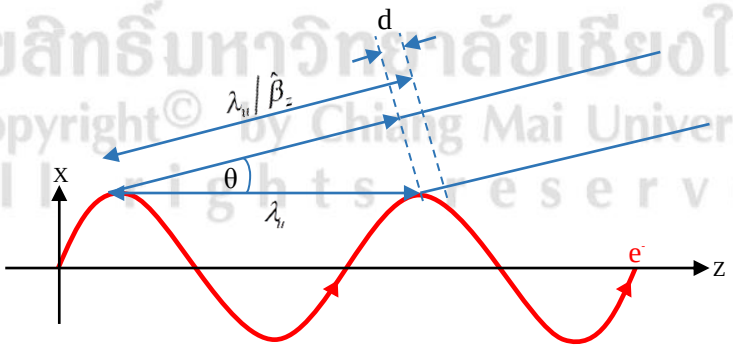

Figure 2.15: The interference effect of the emitted radiation produced from an electron moving in the undulator magnetic field modified from the reference [28].

As shown in Fig. 2.15, the electron travels over one undulator period with time of $\lambda_u / \hat{\beta}_z c$, where $\hat{\beta}_z$ is the average longitudinal velocity of the electron with respect to

the velocity of light [28]. Thus, a distance of the first wave travelling in this time is $\lambda_u / \hat{\beta}_z$. From the constructive interference condition, the different distance of two waves is equal to a harmonic number (n) of radiation wavelengths (λ_r) as

$$n\lambda_r = \frac{\lambda_u}{\hat{\beta}_z} - \lambda_u \cos\theta ,$$

(2.57)

and

$$\hat{\beta}_z \approx 1 - \frac{1}{2\gamma^2} - \frac{K^2}{4\beta\gamma^2} .$$

(2.58)

where the observation angle (θ) is the angle of the emitted radiation relative to the average electron orbit. When inserting Equation (2.58) into Equation (2.57) and using the small angle approximation for the observation angle, the undulator radiation equation becomes

$$\lambda_{r,n} = \frac{\lambda_u}{2n\gamma^2}\left(1 + \frac{K^2}{2} + \theta^2\gamma^2\right).$$

(2.59)

Here, $n = 1, 2, 3, \ldots$ is the harmonic number. The radiation wavelength depends on the undulator period length, the undulator parameter, the electron beam energy, and the observation angle. Since the undulator parameter depends on the peak magnetic field and the undulator period, the radiation wavelength is easily tunable by varying the undulator magnetic field. The observation angle increases when the emitted radiation is observed at the position far away from the average trajectory of the electron and thus the output wavelength gets longer. This phenomenon is called a red shift, which is the result of the Doppler effect between the radiation behind the undulator and the observer.

The characteristics of the radiation can be described with a wavelength spread ($\Delta\lambda_r$) or an undulator bandwidth ($\Delta\lambda_r / \lambda_r$), which is calculated from the interference effect over the whole undulator with a period number (N_u) [28].

$$\frac{\Delta\lambda_r}{\lambda_r} = \frac{1}{1+nN_u} \approx \frac{1}{nN_u}. \tag{2.60}$$

Similarly, the angular spread ($\Delta\theta$) of the undulator radiation is given by

$$\Delta\theta = \sqrt{\frac{2\lambda_r}{N_u\lambda_u}} = \frac{1}{\gamma}\sqrt{\frac{1+K^2/2}{nN_u}}, \tag{2.61}$$

This angular spread covers the observation angle range over non-zero intensity of radiation. Both the radiation bandwidth and the angular spread correspond to a spectral line width of the radiation spectrum, which corresponds to the number of undulator period. When considering the fundamental harmonic ($n=1$) and the undulator parameter of around 1 ($K \approx 1$), the angular spread is about $1/\gamma\sqrt{N_u}$. Therefore, the undulator radiation with many number of periods is collimated in forward direction and has narrow spectral range at a well-specified wavelength. This is the unique property of the undulator radiation. In the case of the electromagnetic undulator, the spectral range of the emitted radiation can be easily varied by adjusting the applied current of the conducting coils of the undulator.

2.7.3 Angular Flux Distribution of Undulator Radiation

As displayed in Fig. 2.16, the observer experiences the undulator radiation with an angle referred to the undulator axis and an angle with respect to the horizontal axis of the observed point (ϕ). The emitted radiation energy (W) per electron per solid angle is proportional to absolute value of the electric field $E(\omega)$ squared as

$$\frac{d^2W}{d\Omega d\omega} = 2\varepsilon_0 cR^2 \left|E(\omega)\right|^2, \tag{2.62}$$

where R is the displacement from the radiated point to the observer, which is supposed to be constant for the far field region.

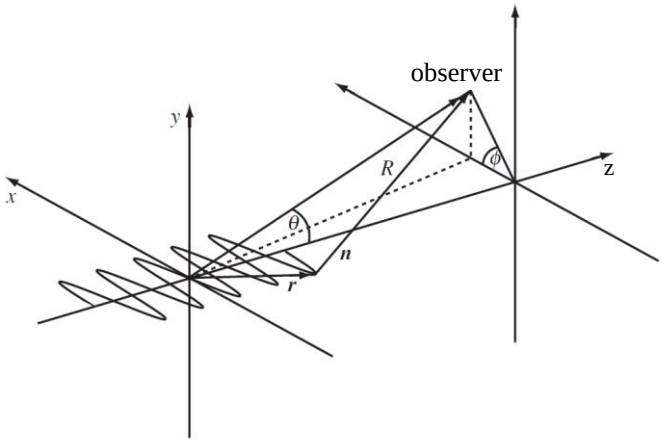

Figure 2.16: Configuration of the undulator radiation with the observation point [28].

For the undulator magnet with N_u periods, the spectral angular energy density is thus defined by

$$\frac{d^2W}{d\Omega d\omega} = \frac{e^2 n^2 N_u^2 \gamma^2}{4\pi\varepsilon_0 cA^2} L_n P_n(K, \gamma\theta, \phi), \tag{2.63}$$

where

$$A = 1 + \frac{K^2}{2} + \theta^2\gamma^2, \tag{2.64}$$

and the Lineshape function is

$$L_n(\lambda_r) = \left[\frac{\sin\left(N_u \pi\Delta\omega/\omega_1\right)}{N_u \sin\left(\pi\Delta\omega/\omega_1\right)}\right]^2 = \left[\frac{\sin\left(N_u \pi\lambda_{r,1}\left(1/\lambda_r - n/\lambda_{r,1}\right)\right)}{N_u \sin\left(\pi\lambda_{r,1}\left(1/\lambda_r - n/\lambda_{r,1}\right)\right)}\right]^2, \tag{2.65}$$

$$P_n(K, \gamma\theta, \phi) = |B|^2 + |B - K(C + D)|^2, \tag{2.66}$$

$$B = 2\gamma\theta \sin(\phi) \sum_{p=-\infty}^{+\infty} J_{n+2p}(X) J_p(Y), \tag{2.67}$$

$$C = \sum_{p=-\infty}^{+\infty} J_{n+2p-1}(X) J_p(Y),$$

(2.68)

$$D = \sum_{p=-\infty}^{+\infty} J_{n+2p+1}(X) J_p(Y),$$

(2.69)

$$X = \frac{2n\gamma\theta K \cos(\phi)}{A},$$

(2.70)

$$Y = \frac{nK^2}{4A},$$

(2.71)

Here, J_p is the Bessel function of the first kind of order p, ω_n is the angular frequency of the n harmonic, which is related to the radiation wavelength as $\omega_n = 2\pi c/\lambda_{r,n}$ and $\Delta\omega$ is equal to $\omega - n\omega_1$.

Each term in Equation (2.63) can be interpreted in different physical meanings. The lineshape function (L_n) explains the interference of the radiated wave from the undulator magnet with N_u periods, which is comparable to the diffraction function of a grating with N_u slits [28]. The lineshape function is equal to 1 at all peaks of the line spectra. Moreover, this function is proportional to the spectral intensity $I(\lambda_r)$ in term of the radiation wavelength as given by [29]

$$I(\lambda_r) \propto \left[\frac{\sin\left(N_u \pi \lambda_{r,1}\left(1/\lambda_r - n/\lambda_{r,1}\right)\right)}{N_u \sin\left(\pi \lambda_{r,1}\left(1/\lambda_r - n/\lambda_{r,1}\right)\right)} \right]^2.$$

(2.72)

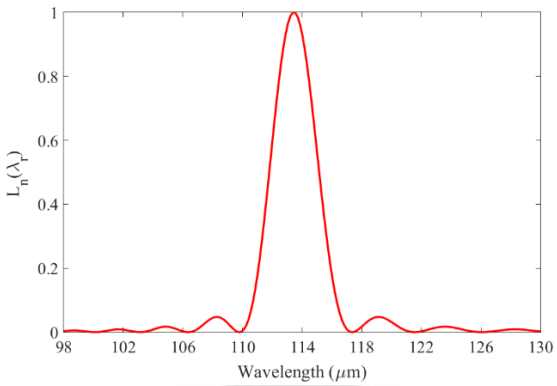

Figure 2.17: Characteristics of the lineshape function $L_n(\lambda_r)$ for the first harmonic.

As an example, the characteristic of the lineshape function of the first harmonic radiation $(n=1)$ for the electron beam with kinetic energy of 10 MeV traveling through the undulator magnet of 30 periods with a period length of 64 mm and an undulator parameter equals to 1 is shown in Fig. 2.17. A sharp peak of the lineshape function holds at $\lambda_{r,1}=113.45\mu\text{m}$, which can be calculated from Equation (2.59).

The last term $P_n(K,\gamma\theta,\phi)$ describes the undulator polarization consisting of the vertical polarization $|B|^2$ and the horizontal polarization $|B-K(C+D)|^2$. When considering in the x-z plane ($\phi=0$), the radiation is only polarized horizontally and hence it is the linear polarization. On the other hand, the radiation is elliptically polarized outside the undulator plane of $\phi\neq 0$.

2.7.4 Spectral Power in Central Cone

In this section, we consider only the on-axis undulator radiation with $\theta=0$. This condition leads to the horizontal polarization that is identical to the radiation in the undulator plane ($\phi=0$). Thus, the on-axis undulator spectrum has only odd harmonics. As shown in Fig. 2.18 and Fig. 2.19, the transverse motion of electron oscillating in x direction contributes only odd harmonic radiation while the longitudinal motion of electron oscillating in z direction contributes even harmonic radiation [7]. The difference between odd harmonics and even harmonics can be clearly illustrated regarding to the electron movement with relativistic velocity along the undulator in the laboratory frame and the moving frame.

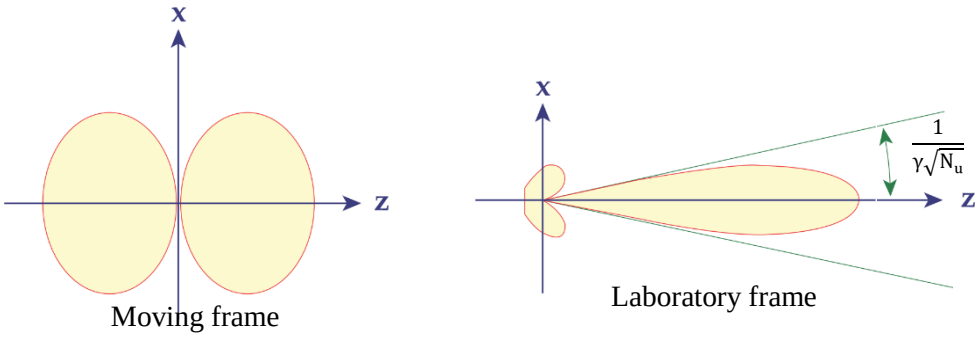

Figure 2.18: The radiation pattern of odd harmonics in the moving frame (left) and the laboratory frame (right) [7].

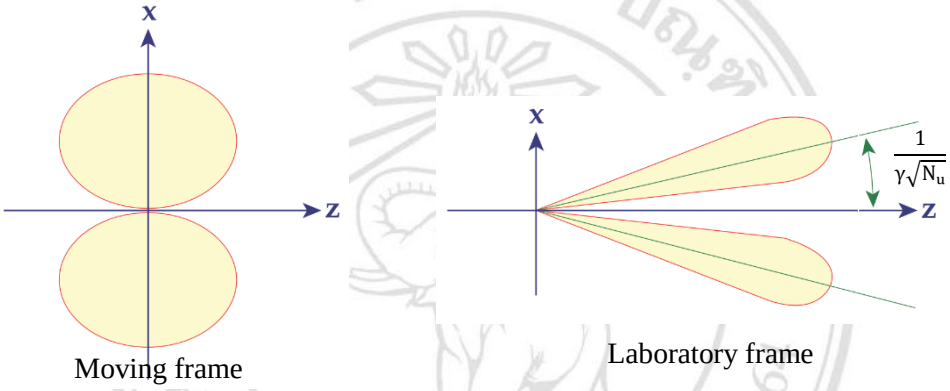

Figure 2.19: The radiation pattern of even harmonics in the moving frame (left) and the laboratory frame (right) [7].

In the moving frame, the electron is accelerated in the x-axis for the transverse motion and in the z-axis for the longitudinal motion. The radiation pattern is similar to a doughnut around the acceleration direction. In the laboratory frame, the radiation field of odd harmonics is concentrated in the forward direction with the opening angle of around $1/\gamma\sqrt{N_u}$. The radiation field is greatly sharp or closely monochromatic when the Lorentz factor and the period number are large. Contradictory, the radiation pattern of even harmonics has two forward cones centered at $1/\gamma\sqrt{N_u}$.

From Equation (2.63), the spectral angular energy distribution in the forward direction for single electron is described by

$$\left.\frac{d^2W}{d\Omega d\omega}\right|_{\theta=0} = \frac{1}{4\pi\varepsilon_0 c}\left(\frac{en\gamma N_u K}{1+K^2/2}\right)^2 L_n F_n,$$

(2.73)

where $F_n = \left(J_{(n+1)/2}(Z) - J_{(n-1)/2}(Z)\right)^2,$

(2.74)

and $$Z = \frac{nK^2}{4\left(1+K^2/2\right)} = \frac{1}{4\gamma^2\lambda_r}\left(2n\gamma^2\lambda_r - \lambda_u\right).$$

(2.75)

Here, F_n is the multiplicative factor related with the radiated power transferred from the fundamental harmonic to the higher harmonics. This factor is defined by the difference of the Bessel function [30]. After integrating over all angles in a specific angular frequency bandwidth ($\Delta\omega$), the spectral energy can be written as

$$W_{1e} = \frac{N_u\omega\lambda_r}{2\varepsilon_0 c\lambda_u}\left(\frac{en\gamma K}{1+K^2/2}\right)^2\left(\frac{\Delta\omega}{\omega}\right)L_n F_n.$$

(2.76)

This equation can be written as a function of the radiation wavelength by using the undulator radiation equation in Equation (2.59) [30]. The on-axis radiated energy for a single electron becomes

$$W_{1e}(\lambda_r) = \frac{\pi e^2 N_u\left(2n\gamma^2\lambda_r - \lambda_u\right)}{2\varepsilon_0\gamma^2\lambda_r^2}\left(\frac{\Delta\omega}{\omega}\right)L_n F_n.$$

(2.77)

2.7.5 Coherent Radiation

The coherent property of any radiation often depends on the properties of its source. In general, the radiation emitted from relativistic electrons experiencing periodic fields is considered as coherent radiation when the electron bunch length is equal or shorter than the radiation wavelength. The coherence radiation is categorized into two types; the temporal and the spatial coherence.

The temporal coherence occurs when the phase difference between two considered points along the direction of propagation is constant. It is determined by a coherence length (l_c) defined by [31]

$$l_c = \frac{\lambda_r^2}{2\pi\Delta\lambda_r} = \frac{(1+nN_u)\lambda_r}{2\pi} \approx \frac{nN_u\lambda_r}{2\pi}, \quad (2.78)$$

where $\Delta\lambda_r$ is from Equation (2.60). As an example, THz radiation with a fundamental wavelength ($n=1$) of about 100 - 1000 μm produced from the 30-period undulator magnet is considered. According to Equation (2.78), the coherence length of this considered case is in the range of 480 - 4800 μm or equivalent to 16 - 160 fs.

The spatial coherence appears when the phase difference between two points in a plane normal to the propagated direction is constant with time. Undulator radiation is considered as spatially coherent radiation when the transverse beam emittance is equal to or less than the diffracted-limited emittance of the photon ($\varepsilon_{ph,diffract}$), which is expressed as [31]

$$\varepsilon_{ph,diffract} = \sigma_r\sigma_{r'} = \frac{\lambda_r}{4\pi}, \quad (2.79)$$

where $\sigma_r = \sqrt{\lambda L}/4\pi$ is the spatial source size, $\sigma_{r'} = \sqrt{\lambda_r / L}$ is the radiation divergence and L is the total length of the undulator magnet, which is derived from $\lambda_u N_u$. This equation reveals that short wavelength radiation matches with low emittance electron beam. As an example, in order to achieve the spatial coherence of the emitted radiation the transverse emittance of the electron beam should not exceed the diffracted-limited emittance of 8 to 80 mm.mrad, which is related to the THz wavelength between 100 μm and 1000 μm.

The total radiated energy (W_{tot}) depending on the radiation energy of a single electron, the number of electrons per bunch, and the bunch form factor $f(\omega)$ is written as [32]

$$W_{tot} = W_{1e} N_e \left[1 + \left(N_e - 1\right) f(\omega)\right].$$

(2.80)

The first term in the brackets describes the incoherent radiation, while the second term determines the coherent one. When the electron bunch length is equal or shorter than the radiation wavelength, the total radiated power of the coherent radiation is proportional to the electron number squared. The form factor $f(\omega)$ is associated with the electron bunch distribution. In our study, we estimated the longitudinal distribution of electron bunch to be the Gaussian distribution with a standard deviation of ($\sigma_x, \sigma_y, \sigma_z$). Thus, three-dimensional bunch form factor is [33]

$$f(\omega) = e^{-(\omega\sigma_x/c)^2} e^{-(\omega\sigma_y/c)^2} e^{-(\omega\sigma_z/c)^2}.$$

(2.81)

The effect of transverse beam distributions can be excluded from the bunch form factor when the emitted radiation is observed in the forward direction or the transverse beam size at the experimental station is small [31]. Consequently, the on-axis longitudinal Gaussian form factor of the electron beam with bunch length (σ_z) is defined by

$$f(\omega) = e^{-(\omega\sigma_z/c)^2} = e^{-(2\pi\sigma_z/\lambda_r)^2}.$$

(2.82)

The radiated energy in Equation (2.77) can be modified to be a pulse power of a radiation pulse by multiplying with the term $N_b N_e \left(1 + \left(N_e - 1\right) f(\omega)\right)$ and dividing by a time duration of the radiation pulse ($\tau_{rad} = N_u \lambda_u / c$), which is given as

$$P_{pulse}(\lambda_r) = \frac{\pi c e^2}{2\varepsilon_0} \frac{N_b \left(2n\gamma^2 \lambda_r - \lambda_u\right)}{\lambda_u \gamma^2 \lambda_r^2} N_e \left(1 + \left(N_e - 1\right) f(\omega)\right) \left(\frac{\Delta\omega}{\omega}\right) L_n F_n,$$

(2.83)

where N_b is number of micro-bunches per pulse. The radiation pulse width is defined from a time of the radiation propagating through the whole undulator magnet. It is the superposition of the undulator radiation from individual poles in forward direction. The pulse power refers to rate of transferred radiation energy in each pulse. When

multiplying Equation (2.83) by the radiation pulse width (τ_{rad}) and dividing by the repetition time (τ_{rep}) of the RF pulse, we obtain an average power from bunches of N_e electrons in the central cone as a function of the wavelength as

$$P_{average}(\lambda_r) = \frac{\pi e^2}{2\varepsilon_0} \frac{N_u N_b \left(2n\gamma^2 \lambda_r - \lambda_u\right)}{\tau_{rep} \gamma^2 \lambda_r^2} N_e \left(1 + \left(N_e - 1\right) f(\omega)\right) \left(\frac{\Delta\omega}{\omega}\right) L_n F_n ,$$

(2.84)

The average power implies to rate of transferred energy over a period of time and can be directly measured from most measurements. In addition, the average power depends not only on the characteristics of the undulator magnet and the electron beam properties but also on the time structure of the RF system. The ratio of the average power and the pulse power is called a duty cycle, which can be written as

$$\text{Duty Cycle} = \frac{P_{average}}{P_{pulse}} = \frac{\tau_{rad}}{\tau_{rep}} .$$

(2.85)

The duty cycle is the fraction of time which a signal is active during a specified period. Thus, it can be defined as the ratio between the radiation pulse width and the repetition time of the RF wave.

2.7.6 Radiation Brightness

In general, the spectral brightness (B_r) of the undulator radiation is determined to be the number of photons (N_{ph}) per second per unit solid angle ($d\Omega$) per unit area (dA) in a fractional bandwidth ($d\omega/\omega$). It is proportional to emittance of the photon source, which corresponds to effective source sizes (Σ_x, Σ_y) and effective divergences ($\Sigma_{x'}, \Sigma_{y'}$) as [28]

$$B_r = \frac{dN_{ph}/dt}{d\Omega dA\, d\omega/\omega} = \frac{\dot{N}_{ph}}{4\pi^2 \Sigma_x \Sigma_y \Sigma_{x'} \Sigma_{y'}}.$$

(2.86)

Equation (2.86) indicates that the electron beam with high electron density, low energy spread, low transverse emittance and short bunch length are required for generating the coherent undulator radiation with high brightness. The photon flux ($\dot{N}_{ph}$) can be converted from a total power in the central cone by dividing Equation (2.84) with the energy of each photon ($\varepsilon_{ph} = h\omega/2\pi = hc/\lambda_r$). The effective source sizes in horizontal and vertical directions are a quadratic combination of the transverse electron beam sizes (σ_x, σ_y) and the photon source size (σ_r) described by

$$\Sigma_x = \sqrt{\sigma_x^2 + \sigma_r^2},$$

(2.87)

and

$$\Sigma_y = \sqrt{\sigma_y^2 + \sigma_r^2}.$$

(2.88)

Similarly, the effective horizontal and vertical divergences are a quadratic combination of the transverse electron beam divergences ($\sigma_{x'}, \sigma_{y'}$) with the photon divergence with an opening angle, which is given by

$$\Sigma_{x'} = \sqrt{\sigma_{x'}^2 + \sigma_{r'}^2},$$

(2.89)

and

$$\Sigma_{y'} = \sqrt{\sigma_{y'}^2 + \sigma_{r'}^2}.$$

(2.90)

Therefore, the brightness of the undulator radiation depends on the transverse properties of both electron beam and photon beam. Consequently, the brightness can be used to compare different radiation sources.

2.8 Transition Radiation

Relativistic electron bunches produced from the PBP-CMU Linac system was first used to generate THz radiation via a transition radiation technique. This radiation is emitted when electrons passing through the boundary between two different dielectric media [6]. At the PBP-CMU Linac Facility, a thin Al-foil was placed in the electron's path at the experimental station. Then, the radiation is emitted at the interface between vacuum and the Al-foil resulting from an electric field discontinuity at the transition area of the materials with different dielectric constants. The power of the THz transition radiation generated from the considered setup of the PBP-CMU Linac is studied in order to compare the performance of the undulator radiation and the transition radiation.

In this study, we consider that the electron travels from vacuum to a perfect conductor in a normal direction as shown in Fig. 2.20. The spectral angular energy density of the transition radiation can be written as [31]

$$\frac{dW_{TR}}{d\Omega d\omega} = \frac{e^2}{\pi^2 c}\frac{\beta^2 \sin^2(\theta)}{(1-\beta^2\cos^2(\theta))^2}. \quad (2.91)$$

For comparison to the undulator radiation, Equation (2.84) can be written in SI unit as

$$\frac{dW_{TR}}{d\Omega d\omega} = \frac{e^2}{4\pi^3 \varepsilon_0 c}\frac{\beta^2 \sin^2(\theta)}{(1-\beta^2\cos^2(\theta))^2}. \quad (2.92)$$

The emitted radiation from the electron with the traveling path perpendicular to the boundary is polarized on the plane of incident. Integrating Equation (2.92) over the solid angle in the left half space (see Fig. 2.20), we obtain the spectral energy density for a single electron as

$$\frac{dW_{TR}}{d\omega} = \frac{e^2}{8\pi^2 \varepsilon_0 c}\left[\frac{1+\beta^2}{\beta}\ln\left(\frac{1+\beta}{1-\beta}\right)-2\right]. \quad (2.93)$$

This equation is called the backward total radiation and involves with any angles between electron travelling path and the boundary.

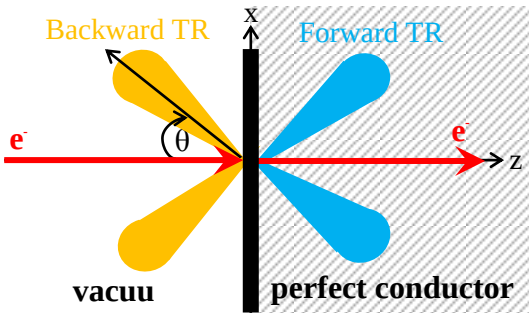

Figure 2.20: Transition radiation of an electron travelling through boundary between vacuum and a perfect conductor.

After integrating Equation (2.93) over a specific angular frequency bandwidth ($\Delta\omega$) and multiplying with the term $N_b N_e \left(1+\left(N_e-1\right) f(\omega)\right)/\tau_{rad}$, the pulse power of the transition radiation in term of the radiation wavelength can be expressed by

$$P_{TR,pulse}(\lambda_r) = \frac{e^2}{4\pi\varepsilon_0}\frac{N_b}{\tau_{rad}\lambda_r} N_e\left(1+\left(N_e-1\right) f(\omega)\right)\left(\frac{\Delta\omega}{\omega}\right)\left[\frac{1+\beta^2}{\beta}\ln\left(\frac{1+\beta}{1-\beta}\right)-2\right]. \quad (2.94)$$

The radiation pulse width (τ_{rad}) of the transition radiation is shorter or equal to the bunch length ($\delta\tau$) of the electron beam because the radiation propagates rapidly across the boundary between vacuum and the Al-foil. When multiplying Equation (2.94) by the duty cycle, the average power of the transition radiation can be expressed as

$$P_{TR,average}(\lambda_r) = \frac{e^2}{4\pi\varepsilon_0}\frac{N_b}{\tau_{rep}\lambda_r} N_e\left(1+\left(N_e-1\right) f(\omega)\right)\left(\frac{\Delta\omega}{\omega}\right)\left[\frac{1+\beta^2}{\beta}\ln\left(\frac{1+\beta}{1-\beta}\right)-2\right]. \quad (2.95)$$

In the experiment, the Al-foil was placed at an angle of 45° with respect to the electron trajectory leading to the backward transition radiation with the radiation direction perpendicular to the electron path. Thus, the emitted radiation in this case consists of both parallel and perpendicular polarization.